Polyhedron 29 (2010) 1130–1136

Contents lists available at ScienceDirect

Polyhedron

journal homepage: www.elsevier.com/locate/poly

Metal derivatives of N^1-substituted thiosemicarbazones with divalent metal ions (Ni, Cu): Synthesis and structures

Tarlok S. Lobana [a,*], Poonam Kumari [a], Geeta Hundal [a], Ray J. Butcher [b]

[a] Department of Chemistry, Guru Nanak Dev University, Amritsar 143 005, India
[b] Department of Chemistry, Howard University, Washington DC 20059, USA

ARTICLE INFO

Article history:
Received 3 October 2009
Accepted 2 December 2009
Available online 21 December 2009

Keywords:
Nickel(II)
Copper(II)
Pyridine-2-carbaldehyde-N^1-methyl thiosemicarbazone
Salicylaldehyde-N^1-phenyl thiosemicarbazone

ABSTRACT

Reactions of nickel(II) acetate with N^1-substituted pyridine-2-carbaldehyde- and salicylaldehyde thiosemicarbazones, $\{R^1(H)C^2{=}N^3{-}N^2(H){-}C^1(=S){-}N^1HR^2\}$, have formed complexes of stoichiometry: (i) $[Ni(\kappa^3\text{-}N^4, N^3, S\text{-}pytscN^1\text{-}R^2)_2]$ $\{R^1 = C_5H_5N, R^2 = Me, \mathbf{1}; Et, \mathbf{2}; Ph, \mathbf{3}\}$ and (ii) $[Ni(\kappa^3\text{-}O, N^3, S\text{-}stscN^1\text{-}R^2)L]$ $\{R^1 = 2\text{-}HOC_6H_4, R^2, L: Me, PPh_3, \mathbf{4}; Et, PPh_3, \mathbf{5}, Me, py, \mathbf{6}; Ph, py, \mathbf{7}\}$. Likewise copper(II) has formed complexes of stoichiometry: $[Cu(\kappa^3\text{-}O, N^3, S\text{-}stscN^1\text{-}R^2)py]$ $\{R^1 = 2\text{-}HOC_6H_4, R^2 = Me, \mathbf{8}; Ph, \mathbf{9}\}$. These complexes have been characterized with the help of analytical data, spectroscopic techniques {IR, ^1H and ^{31}P NMR, electronic absorption} and single crystal X-ray crystallography (**1**, **2**, **4**, **6** and **8**). The complexes have either distorted octahedral (**1–3**) or square planar geometries (**4–9**). The magnetic susceptibility measurements revealed that complexes **1**–**3**, **8** and **9** are paramagnetic.

1. Introduction

Thiosemicarbazones ($R^1R^2C^2{=}N^3{-}N^2(H){-}C(=S)N^1R^3R^4$), a class of Schiff bases, have exhibited variable donor properties, structural diversity and catalytical, analytical and biological applications [1]. The formation of mono-, di- and poly-nuclear complexes including cyclometallation has been observed [1–3]. Among transition metals, thiosemicarbazone complexes of nickel(II) and copper(II) have been more intensively studied, as some of them have shown anticancer, antifungal and antibacterial activities [4–8]. For example, a nickel(II) complex with phenanthrenequinone thiosemicarbazone was tested on human breast cancer cell line, T47D, rich in the progesterone receptors and has a synergistic effect on the antiproliferative activity of the cell line [9]. There are limited Ni^{II}/Cu^{II} complexes reported with N^1-substituted thiosemicarbazones [10–14].

Recently, the influence of the substituents at N^1 nitrogen of fuarn-2-carbaldehyde thiosemicarbazones $\{(C_4H_3O){-}C(H){=}N^3{-}N^2H{-}C^1(=S)N^1HR$, Hftsc; N^1 = Me, Et, Ph$\}$ on the geometry of nickel(II) complexes was investigated [15]. Here, a *cis* square planar complex for phenyl substituent at N^1 nitrogen, and *trans* square planar complexes for methyl and ethyl substituents were obtained. In continuation, to further investigate the effect of the substituents at N^1 nitrogen and C^2 carbon atoms on the nature of complexes with various thiosemicarbazones, the ligands shown in Chart 1 have been used for the preparation of complexes reported in this paper.

2. Materials and techniques

Pyridine-2-carbaldehyde, salicylaldehyde, N^4-methyl thiosemicarbazide, N^4-ethyl thiosemicarbazide, N^4-phenyl thiosemicarbazide, Ph_3P, pyridine, $Ni(OAc)_2$ and $Cu(OAc)_2$ were procured from Aldrich Sigma Ltd. The thiosemicarbazone ligands were prepared by the condensation of a suitable thiosemicarbazides with aldehydes in methanol by refluxing for about 7–8 h [16]. Elemental analysis for C, H and N were carried out using a thermoelectron FLASHEA1112 analyzer. The melting points were determined with a Gallenkamp electrically heated apparatus. The electronic absorption spectra were recorded using UV-1601PC Shimadzu spectrophotometer. Magnetic susceptibility was recorded using magnetic balance procured from Johnson Matthey, Catalytic Systems Division Equipment. The IR spectra were recorded using KBr pellets on a Pye–Unicam SP3-300 spectrophotometer. The ^1H NMR spectra were recorded on a JEOL AL300 FT spectrometer at 300 MHz in $CDCl_3$ with TMS as the internal reference. The ^{31}P spectra were recorded on an AL – 300 FT JEOL spectrometer operating at a frequency of 121.5 MHz, using $CDCl_3$ with *o*-phosphoric acid as the external reference.

* Corresponding author. Tel.: +91 183 2 257604; fax: +91 183 2 258820.
E-mail address: tarlokslobana@yahoo.co.in (T.S. Lobana).

0277-5387/$ - see front matter © 2009 Published by Elsevier Ltd.
doi:10.1016/j.poly.2009.12.013

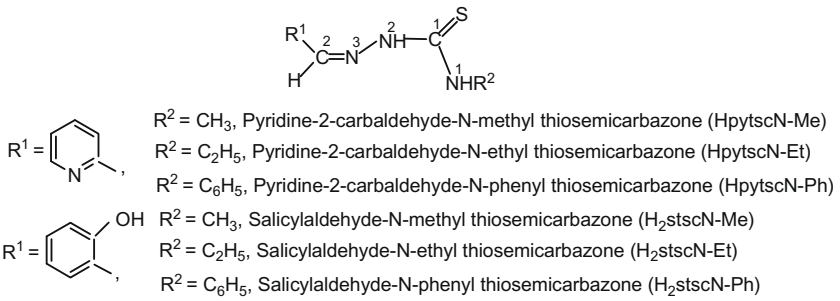

Chart 1. Ligands used.

2.1. Synthesis of complexes

2.1.1. [Ni(κ^3-N^4, N^3, S-pytscN-Me)$_2$]·H_2O (**1**)

To a suspension of HpytscN-Me ligand (0.039 g, 0.200 mmol) in acetonitrile (15 mL) was added solid $Ni(OAc)_2$ salt (0.025 g, 0.100 mmol), and contents were refluxed for 5 h and the red compound formed during refluxing was crystallized from acetonitrile and dichloromethane (3:1: v/v). M.p. 292–294 °C, Yield: 56%. *Anal.* Calc. for $C_{16}H_{20}NiN_8S_2O$: C, 41.45; H, 4.32; N, 24.18. Found: C, 41.87; H, 4.08; N, 24.40%. Main IR peaks (KBr, cm^{-1}), ν(N–H), 3233s, ν(C–H), 3015w, 2928w, 2878w, ν(C=N) + ν(C=C), 1601s, 1514s, ν(C–N), 1099s, 1038s, ν(C–S) 836s. Magnetic moment, μ_{eff} = 2.98 BM.

Complexes **2** and **3** were prepared similarly.

2.1.2. [Ni(κ^3-N^4, N^3, S-pytscN-Et)$_2$] (**2**)

M.p. above 300 °C, Yield, 59%. *Anal.* Calc. for $C_{18}H_{22}N_8NiS_2$: C, 45.64; H, 4.65; N, 23.67. Found: C, 45.59; H, 5.01; N, 23.75%. Main IR peaks (KBr, cm^{-1}), ν(N–H) 3238s, ν(C–H) 3053w, 2974w, 2928w, 2868w, ν(C=N) + ν(C=C) 1601s, 1510s, ν(C–N), 1087s, 1047s, 923w, ν(C–S), 824s. Magnetic moment, μ_{eff} = 3.02 BM.

2.1.3. [Ni(κ^3-N^4, N^3, S-pytscN-Ph)$_2$] (**3**)

M.p. above 300 °C, Yield, 61%. *Anal.* Calc. for $C_{26}H_{22}N_8NiS_2$: C, 54.81; H, 3.86; N, 19.67. Found: C, 54.65; H, 4.18; N, 19.51%. Main IR peaks (KBr, cm^{-1}), ν(N–H) 3263s, ν(C–H) 3055w, 3022w, 2888w, ν(C=N) + ν(C=C) 1589s, 1518s, ν(C–N), 1128s, 1028w, ν(C–S) 894s. Magnetic moment, μ_{eff} = 3.13 BM.

2.1.4. [Ni(κ^3-O, N^3, S-stscN-Me)(PPh_3)] (**4**)

To a solution of H_2stscN-Me (0.021 g, 0.100 mmol) in methanol was added solid $Ni(OAc)_2$ salt (0.025 g, 0.100 mmol) and stirred. The rust colored precipitates formed during stirring were filtered and allowed to dry at room temperature. The analytical data supported the formation of compound of empirical composition, [Ni(stscN-Me)] {*Anal.* Calc. for $C_9H_9NiN_3OS$: C, 40.65; H, 3.39; N, 15.81. Found: C, 40.84; H, 3.23; N, 15.75%}. To a suspension of [Ni(stscN-Me)] (0.025 g, 0.094 mmol) in CH_3CN was added PPh_3 (0.025 g, 0.094 mmol), and contents were stirred for 1 h. The clear solution obtained was allowed to evaporate at room temperature which yielded red colored crystals. M.p. 180–82 °C, Yield, 57%. *Anal.* Calc. for $C_{27}H_{24}NiN_3OPS$: C, 61.34; H, 4.54; N, 7.95. Found: C, 61.56; H, 4.39; N, 7.89%. Main I.R peaks (KBr, cm^{-1}), ν(N–H) 3428s, ν(C–H) 3070w, 3047w, 2887w, 2885w, ν(C=N) + ν(C=C) 1607s, 1528s, ν(P–C) 1097s, ν(C–N), 1024s, 1001s, 916s, ν(C–S) 829s. ^{1}H NMR (δ, $CDCl_3$), δ = 8.34 (d, 1H, C^2H), 7.79 (m, 6H, *o*-H), 7.46 (m, 9H, *p*-H + *m*-H), 7.24 (dd, 1H, C^5H), 7.06 (t, 1H, C^6H), 6.59 (t, 1H, C^8H), 6.41 (d, 1H, C^7H), 4.74 (d, br, 1H, N^1H), 2.90 (d, 3H, CH_3) ppm. ^{31}P NMR ($CDCl_3$), δ = −88.04 ppm. $\Delta\delta(\delta_{complex} - \delta_{PPh3})$ = 25.11 ppm.

Compounds **5**–**9** were prepared similarly.

2.1.5. [Ni(κ^3-O, N^3, S-stscN-Et)(PPh_3)] (**5**)

M.p. 198–200 °C, Yield, 53%. *Anal.* Calc. for $C_{28}H_{26}NiN_3OPS$: C, 61.85; H, 4.97; N, 7.73. Found: C, 62.12; H, 4.67; N, 7.95%. Main IR peaks (KBr, cm^{-1}), ν(N–H) 3420s, ν(C–H) 3078w, 3055w, 2976w, 2929w, ν(C=N) + ν(C=C) 1600s, 1541s, ν(P–C) 1097s, ν(C–N), 1045 m, 1026 m, 920 m, ν(C–S) 841br. ^{1}H NMR (δ, $CDCl_3$), δ = 8.32 (d, 1H, C^2H), 7.80 (m, 6H, *o*-H), 7.44 (m, 9H, *p*-H + *m*-H), 7.26(d, 1H, C^5H), 7.07(t, 1H, C^6H), 6.60 (t, 1H, C^8H), 6.41 (d, 1H, C^7H), 4.71 (s, br, 1H, N^1H), 3.31 (m, 2H, CH_2), 1.13 (t, 3H, CH_3) ppm. ^{31}P NMR ($CDCl_3$), δ = −120.37 ppm. $\Delta\delta(\delta_{complex} - \delta_{PPh3})$ = 25.29 ppm.

2.1.6. [Ni(κ^3-O, N^3, S-stscN-Me)(py)] (**6**)

M.p. 192–94 °C, Yield, 69%. *Anal.* Calc. for $C_{14}H_{14}NiN_4OS$: C, 48.69; H, 4.06; N, 16.23. Found: C, 48.52; H, 4.21; N, 16.15%. Main IR peaks (KBr, cm^{-1}), ν(N–H) 3221s, ν(C–H) 3084w, 3020w, 2988w, ν(C=N) + ν(C=C) 1603s, 1524s, ν(C–N), 1070s, 1022s, 943s, ν(C–S) 829s. ^{1}H NMR (δ, $CDCl_3$), δ = 8.82 (s, 1H, *o*-H(py)), 7.88 (s, 1H, C^2H), 7.44 (t, 1H, *p*-H(py)), 7.31 (t, 2H, *m*-H(py)), 7.18 (m, 2H, C^5H + C^6H), 6.85(d, 1H, C^8H), 6.63(t, 1H, C^7H), 4.61(d, 1H, N^1H), 2.90(d, 3H, CH_3).

2.1.7. [Ni(κ^3-O, N^3, S- stscN-Ph)(py)] (**7**)

M.p. above 300 °C, Yield, 61%. *Anal.* Calc. for $C_{26}H_{22}N_8NiS_2$: C, 54.81; H, 3.86; N, 19.67. Found: C, 54.65; H, 4.08; N, 19.51%. Main IR peaks (KBr, cm^{-1}), ν(N–H) 3264br, ν(C–H) 3053w, 3014w, 2833w, ν(C=N) + ν(C=C) 1602s, 1544s, ν(C–N), 1091s, 1022s, 912s, ν(C–S) 839s. ^{1}H NMR (δ, $CDCl_3$), δ = 8.84 (s, br, 2H, *o*-H(py)), 8.06 (s, 1H, C^2H), 7.77 (t, 1H, *p*-H(py)), 7.47 (d, 2H, *o*-H(Ph)), 7.24 (m, 6H, N^1H + *m*-H(py) *p*-H + *m*-H(Ph)), 6.99(t, 1H, C^5H), 6.88(d, 1H, C^8H), 6.65(t, 1H, C^7H).

2.1.8. [Cu(κ^3-O, N^3, S-stscN-Me)(py)] (**8**)

M.p. 244–46 °C, Yield, 62%. *Anal.* Calc. for $C_{14}H_{14}N_4CuOS$: C, 48.01; H, 4.00; N, 16.00. Found: C, 48.30; H, 4.23; N, 15.96%. Main IR peaks (KBr, cm^{-1}), ν(N–H) 3229s, ν(C–H) 3081w, 3018w, 2977w, 2883w, ν(C=N) + ν(C=C) 1600s, 1558s, ν(C–N), 1070s, 1028s, 912s, ν(C–S) 821s. Magnetic moment, μ_{eff} = 1.80 BM.

2.1.9. [Cu(κ^3-O, N^3, S-stscN-Ph)(py)] (**9**)

M.p. 212–14 °C, Yield, 58%. *Anal.* Calc. for $C_{25.66}H_{31.64}CuN_5O_{3.66}S$: C, 54.57; H, 5.61; N, 12.40. Found: C, 54.46; H, 5.64; N, 12.26%. Main IR peaks (KBr, cm^{-1}), ν(N–H) 3249s, ν(C–H) 3045s, 2988w, 2920w, ν(C=N) + ν(C=C) 1610s, 1533s, ν(C–N) 1067s, 1022s, 946s, ν(C–S) 849s. Magnetic moment, μ_{eff} = 1.82 BM.

2.1.10. ^{1}H NMR spectra of ligands: H_2stscN-Me

^{1}H NMR (δ, $CDCl_3$), δ = 10.95 (s, 1H, OH), 9.61 (s, 1H, N^2H), 8.23 (s, 1H, C^2H), 7.56 (s, br, N^1H), 7.36 (dd, 1H, C^5H), 7.26 (t, 1H, C^6H), 6.90 (m, 2H, C^7H + C^8H), 3.12 (d, 3H, CH_3) ppm. *H_2stscN-Et*, ^{1}H NMR (δ, $CDCl_3$), δ = 10.73 (s, 1H, OH), 9.68 (s, 1H, N^2H), 8.18 (s, 1H, C^2H),

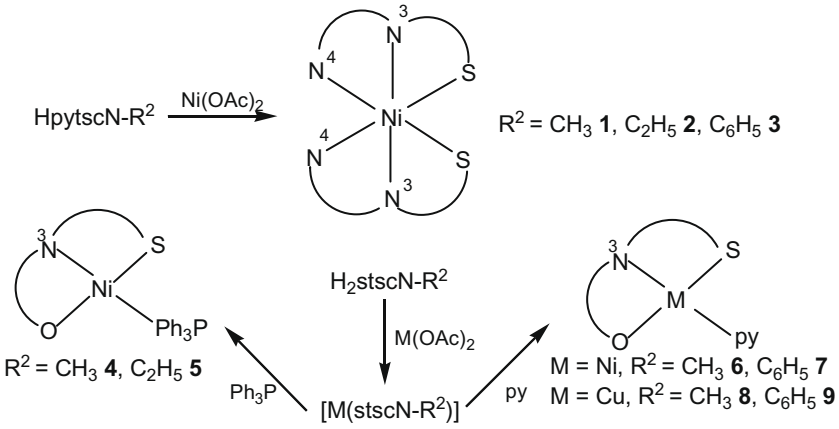

Scheme 1. Synthesis of complexes.

7.30 (m, 2H, $C^5H + C^6H$), 7.08 (s, br, 1H, N^1H), 6.91 (m, 2H, $C^7H + C^8H$), 3.31 (m, 2H, CH_2), 3.74 (m, 2H, CH_2), 1.28 (t, 3H, CH_3) ppm. *H_2stscN-Ph*, ^{1}H NMR (δ, $CDCl_3$), δ = 10.97 (s, 1H, OH), 9.61 (s, 1H, N^2H), 8.95 (s, 1H, N^1H), 8.27 (s, 1H, C^2H), 7.59 (d, 2H, *o*-H(Ph), 7.39 (m, 3H, *m*-H + *p*-H(Ph)), 7.27 (m, 2H, $C^5H + C^6H$), 6.93 (q, 2H, $C^7H + C^8H$).

3. X-ray crystallography

The single crystals of compounds were mounted on Bruker AXS SMART APEX CCD (**1**, **6**, **8**), Oxford Diffraction Gemini (**2**), and Siemens P4 X-ray (**4**) diffractometers, each equipped with a graphite monochromator and Mo Kα radiation (λ = 0.71073 Å) [17–20] (see Supplementary data).

4. Results and discussion

4.1. Synthesis, magnetism and IR spectra

Scheme 1 depicts the formation of complexes **1**–**9** with a series of the thiosemicarbazone ligands. The addition of two equivalents of HpytscN-R^2 ligand to a solution of $Ni(OAc)_2$ in methanol yielded complexes of stoichiometry, [Ni(κ^3-N^4, N^3, S-pytscN-R^2)] {R^2 = Me, **1**; Et, **2**; Ph, **3**}. Similar reactions of $Ni(OAc)_2$/$Cu(OAc)_2$ with H_2stscN-R^2 yielded insoluble compounds of stoichiometry, [M(stscN-R^2)] {M = Ni, Cu; R^2 = CH_3, C_2H_5, C_6H_5}, which after reactions with Ph_3P or py gave crystalline compounds, [M(κ^3-O, N^3, S-stscN^1-R^2)L] {M, R^2, L: Ni, Me, PPh_3, **4**; Ni, Et, PPh_3, **5**; Ni, Me, py, **6**; Ni, Ph, py, **7**; Cu, Me, py, **8**; Cu, Ph, py, **9**}. Complexes with 2-hydroxy phenyl substituent at C^2 carbon of thiosemicarbazones were insoluble and addition of triphenylphosphine or pyridine solubilized them and hence gave good crystals for study (**4**–**9**). The complexes with pyridyl substituent at C^2 carbon were soluble in organic solvents and triphenylphosphine or pyridine did not change the stoichiometry or geometry.

In all these complexes, the thiosemicarbazone ligands are coordinating via X, N^3, S (X = N^4, **1**–**3**; O, **4**–**9**) donor atoms (X-ray crystallography, vide infra). In complexes **1**–**3**, HpytscN-R^2 ligands are uninegative (deprotonation of –N^2H) and in complexes **4**–**9**, the H_2stscN-R^2 ligands are dinegative (deprotonation of –N^2H and –OH). The room temperature magnetic moments, μ_{eff} = 2.98 (**1**), 3.02 (**2**), 3.13 (**3**) BM support high spin nickel(II) octahedral

Table 1
Crystallographic data for complexes **1**, **2**, **4**, **6** and **8**.

	1	**2**	**4**	**6**	**8**
Empirical formula	$C_{16}H_{19}N_8NiOS_2$	$C_{18}H_{22}N_8NiS_2$	$C_{27}H_{24}N_3NiOPS$	$C_{14}H_{14}N_4NiOS$	$C_{14}H_{14}CuN_4OS$
Formula weight	463.23	473.27	528.23	345.06	349.91
T (K)	100(2)	200(2)	295(2)	100(2)	100(2)
Crystal system	monoclinic	monoclinic	triclinic	triclinic	triclinic
Space group	$P2_1/n$	P_12_1/n_1	$P2_1/n$	$P\bar{1}$	$P\bar{1}$
Unit cell dimensions (mm^3)	0.5 × 0.26 × 0.11	0.53 × 0.47 × 0.25	0.20 × 0.20 × 0.10	0.51 × 0.26 × 0.11	0.27 × 0.10 × 0.04
a (Å)	13.3482(8)	9.3015(4)	9.372(1)	5.4014(3)	5.1251(19)
b (Å)	10.7234(6)	13.3920(6)	10.267(2)	8.4760(4)	9.099(3)
c (Å)	14.5093(9)	17.0488(8)	14.680(2)	15.3007(8)	15.117(6)
α (°)	90	90	71.99(1)	99.8020(10)	97.837(5)
β (°)	108.0920(10)	94.199(4)	78.95(1)	93.1620(10)	92.680(5)
γ (°)	90	90	67.74(1)	92.3570(10)	92.932(6)
V (Å^3)	1974.2(2)	2117.99(16)	1238.8(3)	688.31(6)	696.4(4)
Z	4	4	2	2	2
D_{calc} (mg m^{-3})	1.555	1.484	1.416	1.665	1.669
μ (mm^{-1})	1.220	1.135	0.957	1.564	1.721
Reflections collected	17837	18515	4855	7140	6894
Unique reflections	4896 [R(int) = 0.0223]	6929 [R(int) = 0.0657]	4533 [R(int) = 0.0305]	3399 [R(int) = 0.0155]	3395 [R(int) = 0.0369]
Reflections with [$I > 2\sigma(I)$]	4633	3923	2593	3164	2815
R indices (all data)	R_1 = 0.0285, wR_2 = 0.0696	R_1 = 0.1343, wR_2 = 0.1562	R_1 = 0.1327, wR_2 = 0.2654	R_1 = 0.0311, wR_2 = 0.0752	R_1 = 0.0658, wR_2 = 0.1458
Final R indices [$I > 2\sigma(I)$]	R_1 = 0.0269, wR_2 = 0.0682	R_1 = 0.0772, wR_2 = 0.1562	R_1 = 0.0815, wR_2 = 0.2254	R_1 = 0.0288, wR_2 = 0.0733	R_1 = 0.0539, wR_2 = 0.1356

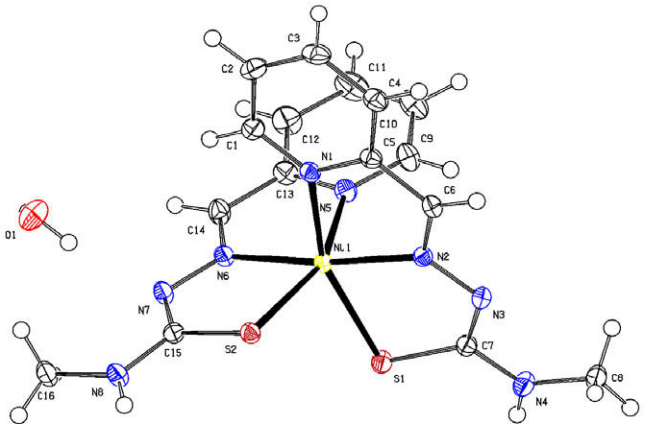

Fig. 1. Molecular structure of complex [Ni(pytscN-Me)$_2$]·H$_2$O (**1**).

complexes. Similarly, magnetic moments (μ_{eff}) of copper(II) complexes **8** and **9** {1.80, 1.84 BM, respectively} are close to the spin-only value of 1.73 BM for d^9 system, Cu(II) [21].

The ligands show IR bands due to $\nu(N^1–H)$, $\nu(N^2–H)$ and ν(O–H) moieties in the region 3432–3249 cm^{-1} and in complexes, the $\nu(N^2–H)$ (**1**–**9**) as well as the ν(O–H) (**4**–**9**) bands disappear. This reveals that the ligands are coordinated to the metal center in the anionic forms. The diagnostic ν(C–S) bands lie in the range, 841–821 cm^{-1} in the complexes (cf. free ligands, 899–867 cm^{-1}). The presence of PPh_3 is confirmed by their characteristic ν(P–C) bands at 1096 and 1097 cm^{-1} in **4** and **5**, respectively.

4.2. Structures of complexes

The detailed structural parameters of complexes **1**, **2**, **4**, **6** and **8** are given in Table 1. The selected bond angles and bond lengths are listed in Table 2.

4.3. Octahedral complexes

The atomic numbering scheme for complex [Ni(pytscN-Me)$_2$]·H$_2$O (**1**) is given in Fig. 1. Complex crystallized in the mono-

Table 2
Selected bond lengths and bond angles.

1			
Ni–S(1)	2.422(4)	Ni–N(1)	2.113(12)
Ni–N(2)	2.022(11)	Ni–S(2)	2.437(4)
Ni–N(5)	2.103(12)	Ni–N(6)	2.031(11)
C(6)–N(2)	1.292(18)	C(14)–N(6)	1.291(18)
C(7)–S(1)	1.742(14)	C(15)–S(2)	1.733(14)
N(1)–Ni–N(2)	78.99(5)	N(2)–Ni–S(1)	80.67(3)
N(5)–Ni–N(6)	78.85(5)	N(6)–Ni–S(2)	80.25(3)
S(1)–Ni–S(2)	97.14(13)	N(1)–Ni–N(5)	86.36(5)
N(2)–Ni–N(6)	172.88(4)	N(1)–Ni–S(1)	159.56(3)
N(5)–Ni–S(2)	158.27(3)		
2			
Ni–S(1)	2.409(13)	Ni–N(1)	2.100(4)
Ni–N(2)	2.036(4)	Ni–S(2)	2.413(13)
Ni–N(5)	2.137(4)	Ni–N(6)	2.037(4)
C(6)–N(2)	1.288(5)	C(15)–N(6)	1.293(5)
C(7)–S(1)	1.725(5)	C(16)–S(2)	1.724(4)
N(1)–Ni–N(2)	78.72(14)	N(2)–Ni–S(1)	80.11(11)
N(5)–Ni–N(6)	78.54(14)	N(6)–Ni–S(2)	80.20(11)
S(1)–Ni–S(2)	96.38(4)	N(1)–Ni–N(5)	86.13(14)
N(2)–Ni–N(6)	175.80(14)	N(1)–Ni–S(1)	158.76(11)
N(5)–Ni–S(2)	157.10(11)		
4			
Ni–N(1)	1.879(6)	Ni–O(1)	1.855(6)
Ni–S(1)	2.128(18)	Ni–P(1)	2.186(2)
C(25)–N(1)	1.302(9)	C(26)–S(1)	1.759(7)
N(1)–Ni–S(1)	87.77(18)	P(1)–Ni–S(1)	93.81(8)
O(1)–Ni–N(1)	94.60(3)	P(1)–Ni–O(1)	83.90(2)
O(1)–Ni–S(1)	177.40(2)	P(1)–Ni–N(1)	177.99(18)
6			
Ni–N(1)	1.907(14)	Ni–N(2)	1.856(14)
Ni–S(1)	2.144(5)	Ni–O(1)	1.867(12)
C(12)–N(2)	1.303(2)	C(13)–S(1)	1.745(17)
N(2)–Ni–O(1)	96.64(6)	N(2)–Ni–S(1)	87.64(4)
O(1)–Ni–N(1)	85.62(5)	N(1)–Ni–S(1)	90.10(4)
N(1)–Ni–N(2)	177.73(6)	S(1)–Ni–O(1)	175.71(4)
8			
Cu–N(1)	1.951(3)	Cu–N(4)	2.041(3)
Cu–S(1)	2.257(11)	Cu–O(1)	1.906(2)
C(7)–N(1)	1.302(4)	C(8)–S(1)	1.754(3)
N(1)–Cu–O(1)	95.19(11)	N(4)–Cu–S(1)	93.07(9)
O(1)–Cu–N(4)	86.49(11)	N(1)–Cu–S(1)	85.71(9)
N(1)–Cu–N(4)	175.67(12)	O(1)–Cu–S(1)	173.46(8)

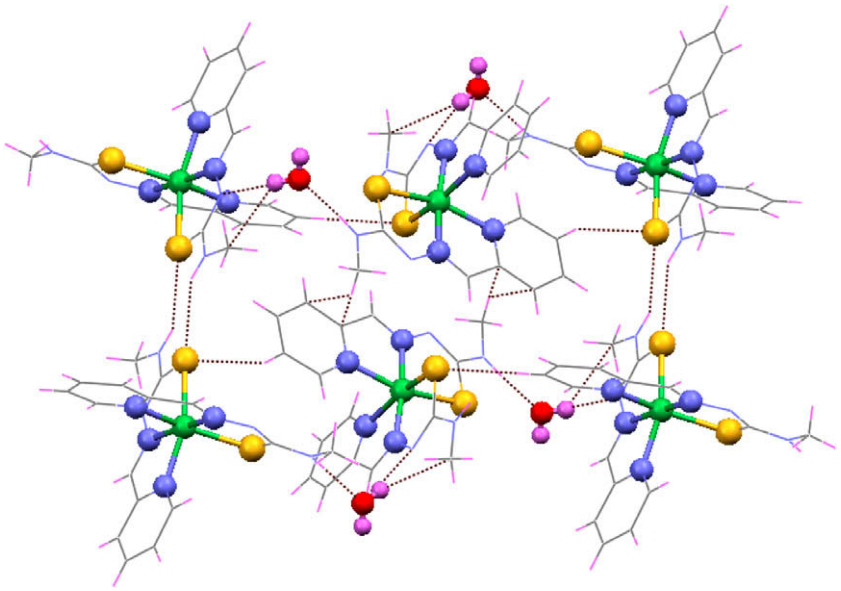

Fig. 2. Packing diagram of complex **1**.

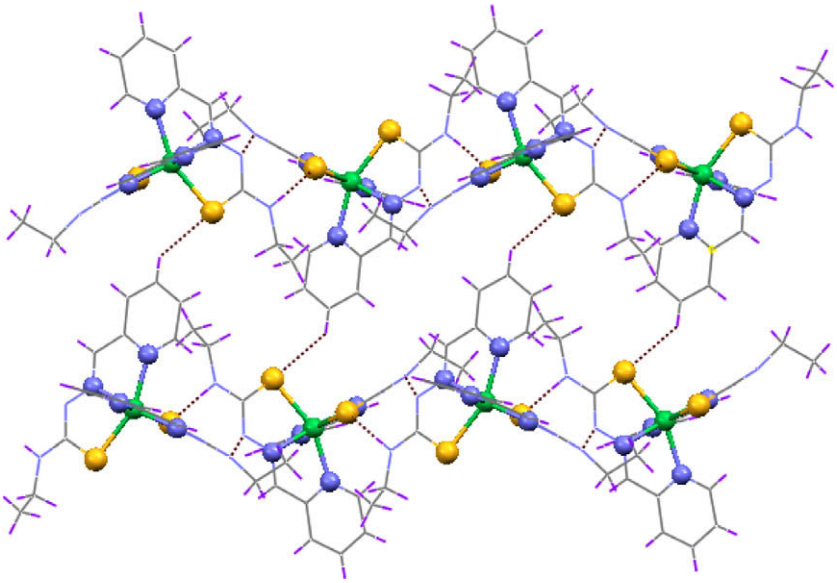

Fig. 3. Packing diagram of complex **2**.

clinic crystal system. In this complex two uninegative pytscN-Me$^-$ moieties are coordinated to nickel with sulfur and pyridyl nitrogen atoms occupying *cis* positions of the octahedron [22]. The azomethine nitrogen atoms are in *trans* positions. The *trans* angles, N(1)–Ni(1)–S(1) {159.56(3)}, N(5)–Ni(1)–S(2) {158.27(3)} and N(2)–Ni(1)–N(6) {172.88(4)°}, suggest considerable distortion from an octahedral geometry around the Ni(II) center (Table 2). The bond parameters are analogous to [NiL_2]·0.5EtOH **10** (L = 2-acetylpyridine thiosemicarbazonate) [23], and [NiL_2] **11** (L = isoquinoline-1-carbaldehyde thiosemicarbazonate) [24]. Further, it was noted that the replacement of methyl group at N^1 nitrogen (HpytscN^1-Me) by ethyl group (HpytscN^1-Et), has also formed similar octahedral complex, [Ni(pytscN-Et)$_2$] **2** with slight variations in the bond parameters compared to complex **1** (Table 2).

An analysis of the packing diagrams of **1** and **2** reveals interesting trends of intermolecular interactions. In complex **1**, water is present in the crystal lattice and is involved in H-bonding, while in **2** there is no water. In complex **1**, the N^1H and CH_3 groups of $-N^1HCH_3$ moiety are engaged in H-bonding with water molecule {$N^1H\cdots OH_2$, 1.99; $H_3C\cdots HOH$, 2.85 Å}, while in complex **2**, the N^1H proton of $-N^1HCH_2CH_3$ moiety is engaged in H-bonding with sulfur atom of thioamide moiety {$C-S\cdots HN^1$, 2.58 Å}, but ethyl group shows no interaction with any electronegative atom. Further, in complex **1**, there are interactions of water with N^2 and CH_3 groups {$HOH\cdots N^2$(hydrazinic), 2.06 Å; $HOH\cdots CH_3$, 2.85 Å}. The oxygen atom of this water molecule further interacts strongly with the adjacent Ni(pytscN-Me)$_2$ molecule via $H_2O\cdots HN^1$ interaction (1.99 Å). Similarly, there is an intermolecular $C-H_{py}\cdots S=C$ (2.78 Å) interaction leading to the formation of a zig-zag polymeric chain. This polymeric chain interacts with another similar polymeric chain via $C-S\cdots HN^1$(2.69 Å), $H_2C-H\cdots\pi$(py, 2.89, 2.87 Å) interactions forming a 2D polymer (Fig. 2).

While in complex **2**, the deprotonated hydrazinic nitrogen, ($-N^2-$) and N^1H hydrogen atom of one Ni(pytscN-Et)$_2$ molecule interacts with the adjacent Ni(pytscN-Et)$_2$ molecule via (hydrazinic)$N^2\cdots HN^1$(substituted amino), and $C-S\cdots HN^1$ interactions (2.25 Å and 2.58 Å, respectively) forming a long polymeric 1D chain. This polymeric chain interacts with another chain via $C-S\cdots\pi$(py) interaction (2.94 Å), and forms a 2D polymer (Fig. 3).

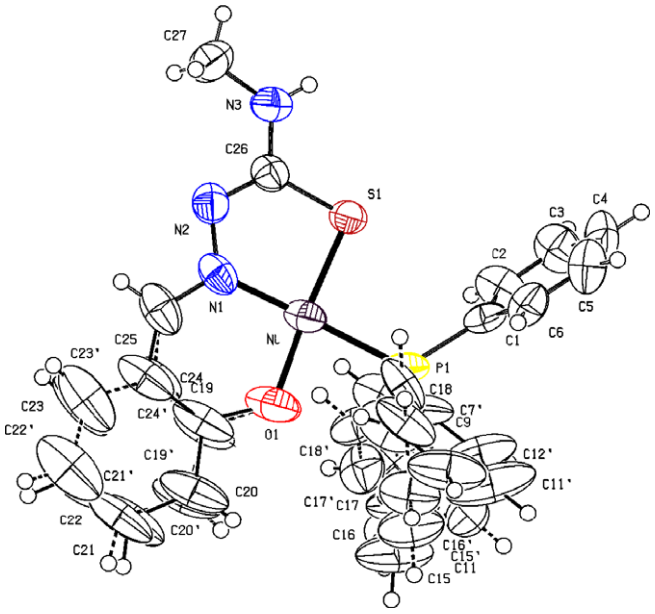

Fig. 4. Molecular structure of complex [Ni(stsc-N-Me)(PPh_3)] (**4**).

4.4. Square planar complexes

The atomic numbering schemes for complexes **4** and **6** are given in Figs. 4 and 5, respectively. Compounds **4** and **6** crystallized in the triclinic system. The molecular structures of complexes, [Ni(stscN-Me)Ph_3P] (**4**) and [Ni(stscN-Me)py] (**6**) have shown that the dinegative thiosemicarbazone ligands (stscN-Me$^-$) bind to the nickel(II) center via O, N^3, S-donor atoms. The fourth coordination site around nickel(II) is occupied by PPh_3 ligand in complex **4** and by pyridine in **6**, forming distorted square planar complexes. In both the complexes, the *trans* angles, {N1–Ni1–P1, 175.71(4); S1–Ni–O1 177.73(6)° **4** and N1–Ni1–N2, 177.73(6); S1–Ni–O1, 175.71(4)° **6**}, are similar and deviate less from linearity. The Ni–P1 bond distance in complex **4** is similar to that in the analogous complex, [Ni(L)(PPh_3)] **12** (L = salicylaldehyde-N-phenylthiosemicarbazone) [25]. The Ni–N1(pyridine) bond distance in complex **6** {1.907(14) Å} is similar to that in the analogous

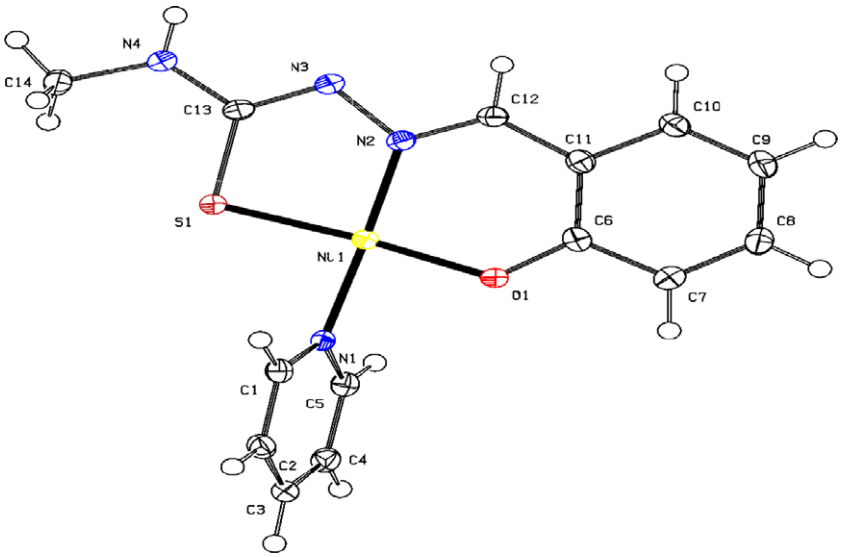

Fig. 5. Molecular structure of complex [Ni(stsc-N-Me)(py)] (**6**).

complex, $[Ni(L)py]NO_3$ (L = pyridoxal thiosemicarbazone) **13** {1.919(21) Å} [26]. Complex, [Cu(stscN-Me)py] (**8**), also has a square planar geometry with the bond distances and angles, similar to that in complex **6** (Table 2).

The packing diagrams of the square planar complexes revealed that the methyl group at N^1 nitrogen is involved in the intermolecular interactions in **4** and **6**. This behavior is similar to that in the octahedral complexes discussed above. In complex **4**, the

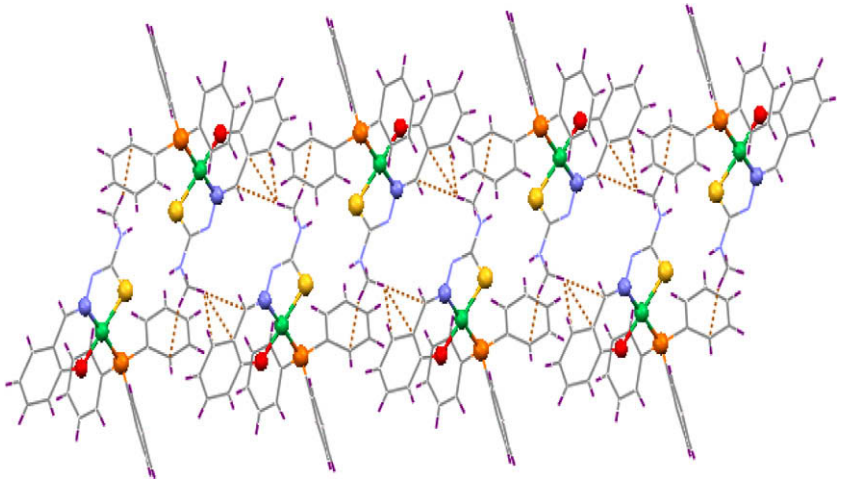

Fig. 6. Packing diagram of complex **4**.

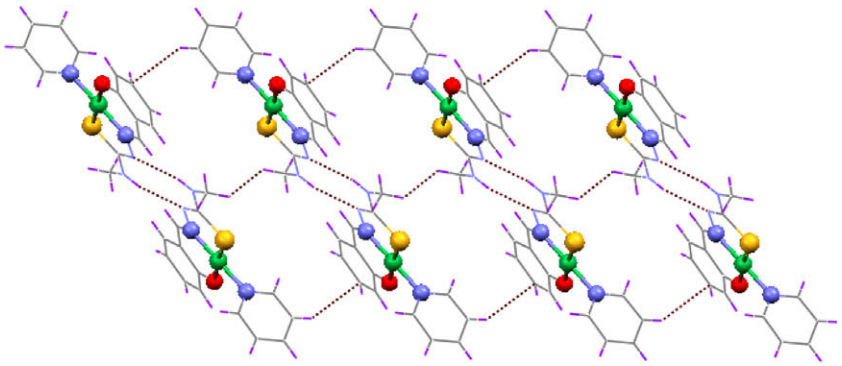

Fig. 7. Packing diagram of complex **6**.

molecules pack in a linear fashion along the *a*-axis with no interactions with the adjacent molecules (Fig. 6). There are inter-chain diagonal interactions between the molecules involving the methyl substituent at N^1 nitrogen {$(CH_3)C–H\cdots\pi$(C=N, azomethine), 2.835; $(CH_3)C–H\cdots\pi(C_6H_4O–)$, 2.815, 2.891; $(CH_3)C–H\cdots\pi$ (Ph–P), 2.826 Å} and form 2D polymeric network. In complex **6**, the molecules interact in a linear fashion along the *a*-axis involving methyl, phenolate and pyridyl groups {$(CH_3)C–H\cdots\sigma$(C–H, CH_3, 2.369 Å); (py)C–H$\cdots\pi$(Ph, 2.895 Å) (Fig. 7).

5. Solution phase studies

The ^{1}H NMR spectra of the diamagnetic complexes (**4**–**7**), revealed that the $–N^2H$ (hydrazinic) and –OH (hydroxyl) moieties were deprotonated. The $–N^1H$-proton signals in complexes are upfield relative to the free ligands {δ: 4.74 (methyl, **4**), 4.61(methyl, **6**); 4.71 (ethyl, **5**) and 7.24 ppm (phenyl, **7**); free ligands' $–N^1H$-protons: 7.56 (H_2stscN-Me), 7.08(H_2stscN-Et) and 8.95 ppm (H_2stscN-Ph)}. This trend is in line with the literature studies [16]. It shows that the position of $–N^1H$- proton signal changes with the nature of the substituent. Finally, the C^2H signals in complexes are downfield (**4**, **5**) or upfield (**6**, **7**) depending on the type of co-ligand (PPh_3 versus py). The ^{31}P NMR spectra showed coordination shifts {$\Delta\delta(\delta_{complex} - \delta_{ligand})$} of 25.11 and 25.29 ppm in complexes **4** and **5**, respectively. These shifts show that the PPh_3 is coordinating relatively strongly [27].

In the N, S-donor ligand, HpytscN-Et, two intense absorption bands at 210 and 319 nm are assigned to $\pi \rightarrow \pi^*$ and $n \rightarrow \pi^*$ transitions, respectively. These bands in complex **2** appear at 226 and 301 nm. Two bands at 342 and 359 nm are assigned to S → Ni charge transfer transitions, while the bands at 800 and 407 nm are assigned to the d–d transitions: $^3A_{2g}(F) \rightarrow {}^3T_{1g}(F)$ and $^3A_{2g}(F) \rightarrow {}^3T_{1g}(P)$, respectively. The various transitions in complexes **1** and **3** are assigned as follows: $\pi \rightarrow \pi^*$ (224, **1**; 209, 255, **3**), $n \rightarrow \pi^*$ (301, **1**; 320, **3**), S → Ni(CT) (345, 362, **1**; 375, **3**), $^3A_{2g}(F) \rightarrow {}^3T_{1g}(P)$ (402, **1**; 420, **3**) and $^3A_{2g}(F) \rightarrow {}^3T_{1g}(F)$ (800 nm, **1**, **3**) [21]. Similarly, in the O, N, S-donor ligand, H_2stscN-Me, the $\pi \rightarrow \pi^*$ (211, 237 nm) and $n \rightarrow \pi^*$ transitions (293, 304, 331 nm) shift to 233 and 301 nm in square planar complex **4**. The S → Ni charge transfer transition in this complex appears to merge with the $^1A_{1g} \rightarrow {}^1E_g$ transition at 363 nm. The band at 409 nm is assigned to $^1A_{1g} \rightarrow {}^1A_{2g}$ transition. Complexes **5–7**, have shown similar transitions in the ranges: 232–266 ($\pi \rightarrow \pi^*$), 302–320 ($n \rightarrow \pi^*$), 364–370 (S → Ni + $^1A_{1g} \rightarrow {}^1E_g$) and 405–414 nm ($^1A_{1g} \rightarrow {}^1A_{2g}$) [27]. In Cu(II) complexes, the transitions occur as follows: $\pi \rightarrow \pi^*$ (293, **8**; 288, **9**), n → π^* + O → Cu (327, **8**; 318, **9**) and S → Cu + $^2B_{1g} \rightarrow {}^2E_g$ (397, **8**; 393, **9**) [28].

6. Conclusion

In this investigation, two types of N^1-subtituted thiosemicarbazone ligands have been used with pyridyl and 2-hydroxy phenyl substituents at C^2 carbon. Pyridyl based ligands act as uninegative tridentate and formed bis-octahedral complexes, while 2-hydroxy phenyl based ligands act as dinegative tridentate and formed square planar complexes. The substituents at N^1 nitrogen did not affect geometry of nickel(II) complexes, however, they influenced the packing arrangements as described in this paper. Here methyl substituent participates in packing while ethyl group showed no interaction. Finally the PPh_3 ligand showed coordination to nickel(II), but did not show any binding to copper(II).

Acknowledgements

Financial assistance from CSIR, New Delhi {Scheme no. 01(1993)/05/EMR II} and research facilities to one of us (Poonam) by the university are gratefully acknowledged. The authors thank Matthias Zeller of Youngstown State University, USA for his useful suggestions and in X-ray crystallography.

Appendix A. Supplementary data

CCDC 747915, 747914, 747916, 747917 and 747913 contain the supplementary crystallographic data for **1**, **2**, **4**, **6** and **8**. These data can be obtained free of charge via http://www.ccdc.cam.ac.uk/conts/retrieving.html, or from the Cambridge Crystallographic Data Center, 12 Union Road, Cambridge CB2 1EZ, UK; fax: (+44) 1223-336-033; or e-mail: deposit@ccdc.cam.ac.uk. Supplementary data associated with this article can be found, in the online version, at doi:10.1016/j.poly.2009.12.013.

References

[1] T.S. Lobana, R. Sharma, G. Bawa, S. Khanna, Coord. Chem. Rev. 253 (2009) 977.
[2] T.S. Lobana, G. Bawa, A. Castineiras, R.J. Butcher, M. Zeller, Organometallics 27 (2008) 175.
[3] T.S. Lobana, G. Bawa, G. Hundal, M. Zeller, Z. Anorg. Allg. Chem. 634 (2008) 931.
[4] J. Garcia-Tojal, J.L. Pizarro, A. Garcia-Orad, A.R. Perez-Sanz, M. Ugalde, A.A. Diaz, J.L. Serra, M.I. Arriortua, T. Rojo, J. Inorg. Biochem. 86 (2001) 627.
[5] M.B. Ferrari, F. Bisceglie, G. Pelosi, P. Tarasconi, R. Albertini, A. Bonati, P. Lunghi, S. Pinelli, J. Inorg. Biochem. 83 (2001) 169.
[6] M.B. Ferrari, F. Bisceglie, G. Pelosi, P. Tarasconi, A. Albertini, P.P. Dall'Aglio, S. Pinelli, A. Bergamo, G. Sava, J. Inorg. Biochem. 98 (2004) 301.
[7] M.A. Ali, A.H. Mirza, A.M.S. Hossain, M. Nazimuddin, Polyhedron 20 (2001) 1045.
[8] M. Joseph, M. Kuriakose, M.R.P. Kurup, E. Suresh, A. Kishore, S.G. Bhat, Polyhedron 25 (2006) 61.
[9] M.B. Ferrari, C. Pelizzi, G. Pelosi, M.C. Rodriguez-Arguelles, Polyhedron 21 (2002) 2593.
[10] D.X. West, G.A. Bain, R.J. Butcher, J.P. Jasinski, Y. Li, R.Y. Pozdniakiv, J. Valdes-Martinez, R.A. Toscano, S. Hernandez-Ortega, Polyhedron 15 (1996) 665.
[11] M. Soriano-Garcia, R.A. Toscano, J. Valdes-Martinez, J.M. Fernanadez, Acta Crystallogr., Sect. C: Cryst. Struct. Commun. 41 (1985) 498.
[12] A. Berkessel, G. Hermann, O.-T. Rauch, M. Buchner, A. Jacobi, G. Huttner, Chem. Ber. 129 (1996) 1421.
[13] J. Valdes-Martinez, S. Hernandez-Ortega, V.B. Jimenez, Acta Crystallogr., Sect. E: Struct. Rep. Online 58 (2002) m710.
[14] J. Valdes-Martinez, S. Hernandez-Ortega, V.B. Jimenez, Acta Crystallallogr., Sect E: Struct. Rep. Online 60 (2004) 42.
[15] T.S. Lobana, P. Kumari, M. Zeller, R.J. Butcher, Inorg. Chem. Commun. 11 (2008) 972.
[16] T.S. Lobana, A. Sanchez, J.S. Casas, A. Castineiras, J. Sordo, M.S. Garcia-Tasende, E.M.V. Lopaz, J. Chem., Soc. Dalton Trans. (1997) 4289.
[17] Bruker, SMART and SAINT. Area Detector Control and Integration Software, Bruker Analytical X-ray Instruments Inc., Madison, Wisconsin, USA, 1997.
[18] G.M. Sheldrick, Acta Crystallogr., Sect. A64 (2008) 112.
[19] WINGX L.J. Farrugia, J. Appl. Crystallogr. 32 (1999) 837.
[20] G.M. Sheldrick, Acta Crystallogr., Sect. A46 (1990) 467.
[21] A.B.P. Lever, Inorganic Electronic Spectroscopy, Elsevier, New York, 1984.
[22] I. Garcia, E. Bermejo, A.K. El Sawaf, A. Castineiras, D.X. West, Polyhedron 21 (2002) 729.
[23] N.C. Kasuga, K. Sekino, C. Koumo, N. Shimada, M. Ishikawa, K. Nomiya, J. Inorg. Biochem. 84 (2001) 55.
[24] M. Mathew, G.J. Palenik, J. Am. Chem. Soc. 91 (1969) 6310.
[25] R. Prabhakaran, R. Karvembu, T. Hashimoto, K. Shimizu, K. Natarajan, Inorg. Chim. Acta 358 (2005) 2093.
[26] V.M. Leovac, L.S. Jovanovic, V. Divjakovic, A. Pevec, I. Leban, T. Armbruster, Polyhedron 26 (2007) 49.
[27] B. Ülküseven, T. Bal-Demirci, M. Akkurt, S.P. Yalçın, O. Büyükgüngör, Polyhedron 27 (2008) 3646.
[28] A. Sreekanth, M.R.P. Kurup, Polyhedron 22 (2003) 3321.